6-DOF DESK-TOP VOICE-COIL JOYSTICK

S.E. Salcudean and **N.R. Parker**
Department of Electrical and Computer Engineering
University of British Columbia
Vancouver, BC, V6T 1Z4, Canada
{ *tims@ee.ubc.ca* }

ABSTRACT

This paper presents the design of a 6-DOF desk-top magnetically levitated force-feedback joystick utilizing voice-coil actuation. Relative to prior designs (Hollis et. al., 1991),(Salcudean et. al., 1995),(Berkelman et. al., 1996), this haptic interface features a novel geometry, a novel optical sensor and optimized actuation. These allow for all the electronics including the control microprocessor to be integrated in its base, with the device tapering from a handle 5.5" high to a footprint of 10.5"×5.5". The device has a maximum translational motion range of ± 3mm limited by the actuation gap, and a predicted maximum rotational motion range of $\pm 5^\circ$ limited by the sensor motion range. The moving mass of 260 grams will have maximum accelerations exceeding 10 g's, and will be able to exert continuous forces as large as 16N.

INTRODUCTION

A number of haptic interface designs have been proposed for virtual environments and teleoperation systems. The reader is referred to prior ASME-DSC volumes, to (Stocco and Salcudean, 1996) for a detailed survey, and to (Hayward and Astley, 1995) for performance measures. The need for high acceleration in haptic interfaces has been demonstrated in many studies and seems to have been accepted by designers. Although most reported designs have translational workspaces that exceed a cube with 10cm sides, it has not been demonstrated that a workspace of this magnitude is really needed. Indeed, for desk-top computing, input devices such as mice, trackballs or joysticks are commonplace, and these devices have relatively small motion ranges to avoid tiring the operator. Furthermore, designing high acceleration devices over large workspaces is a non-trivial task requiring expensive actuators, transmissions and joints. As an alternative, the use of a small workspace haptic device in rate mode or combined position/rate mode has been proposed and demonstrated before (Salcudean et. al., 1995). It has been argued in several papers (see, for example, (Hollis and Salcudean, 1993),(Salcudean et. al., 1995)), that magnetically levitated (maglev) Lorentz devices (Hollis et. al., 1991) are suitable small-motion haptic interfaces because of their low mechanical impedance and high acceleration ability. Devices have been built at IBM (Hollis et. al., 1991), University of British Columbia (Salcudean et. al., 1995), and Carnegie-Mellon University (Berkelman et. al., 1996). With respect to prior maglev designs, the haptic interface presented in this paper has the following novel features: (i) a new cubic geometry leading to a smaller device with a perfectly conditioned transformation from actuator currents to resultant forces, (ii) a new, inexpensive, optical sensor using three linear position-sensing diodes and multiplexed planar infrared light beams, (iii) optimized voice-coil actuators. These features are integrated in a novel way into a device that is the first maglev haptic interface that is inexpensive and small enough to fit on the user's desk by a workstation or PC.

The paper is organized as follows: first, the electromechanical design of this haptic interface is presented. A simple methodology for voice-coil actuator optimization for maximum efficiency is discussed next. Then, the novel optical sensor is presented. Issues related to the control electronics and implementation follow. The paper concludes with the project status and plans for future work.

ELECTROMECHANICAL DESIGN

The photograph of the maglev haptic interface prototype is shown in Figure 1. The user manipulates a mouse-like handle attached to a mobile flotor shown in Figure 2. The flotor

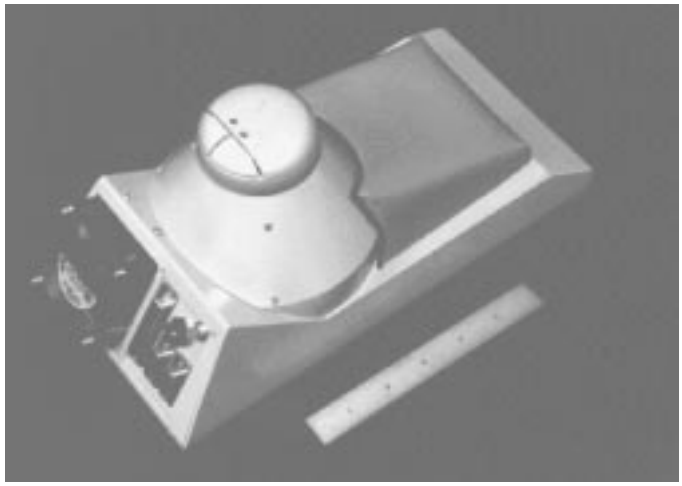

Figure 1: Photograph of the maglev desk-top joystick: a sloped support allows the user to easily grasp the disk-shaped handle.

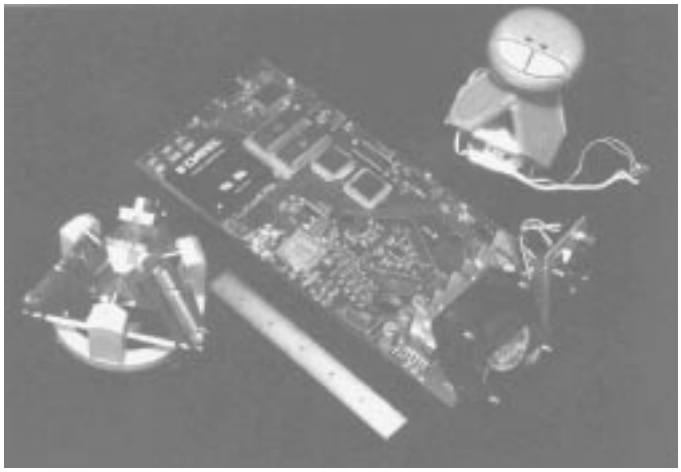

Figure 3: Maglev joystick stator, flotor and controller board.

can move within the confines of a stator that is attached by three mounting posts to a plastic base. A printed circuit board (PCB) fits between the stator and the plastic base and carries the device sensing and power electronics and a microcontroller. A photograph of the main components - stator, flotor and PCB - is shown in Figure 3. The flotor and stator of the device are shown schematically in Figure 4. The basic actuator is the same as used before in a number of designs (Hollis et. al., 1991) and is shown in Figure 5.

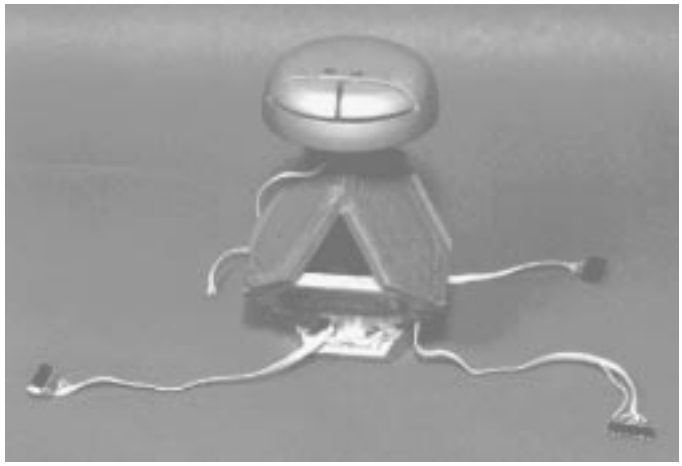

Figure 2: Maglev joystick flotor

Six flat coils fit in the faces of the hollow cubic flotor structure having an outer dimension equal to 53mm, a shell and coil thickness equal to $d_c = 5$mm, and a mass of 190 grams. The coils are oriented along the diagonals of each cube face. Inside the flotor shell, stator magnets matching the coils are arranged on a cubic soft iron core. Outside the flotor shell, magnets matching the coils are mounted on soft-iron return plates arranged in a cubic structure. The magnet dimensions are $l_m = 20$mm, $w_m = 8$mm, $t_m = 4$mm, and the magnetic gap is $d = 11$mm. The magnetic gaps allow the structure to translate ± 3mm in any direction in the absence of rotation. The rotational and translational workspaces do not decouple in this design, unlike in the spherical geometry suggested in (Berkelman et. al., 1996). However, the angular motion of the device is substantial (at least $\pm 10^\circ$) from nominal, and is actually limited by the optical sensor range, not by mechanical interference. Because the flotor coils are arranged along the diagonals of a cube as shown, four of the cube vertices can be cut away. Three of these leave room for support posts to hold the inner cubic structure, and one leaves room for the optical sensor, described later in the paper. A light handle can be mounted on a vertical shaft penetrating the top vertex.

The device modeling follows closely the approach from (Hollis et. al., 1991) and will not be presented in detail. The flotor is represented schematically in Figure 6. In the nominal position, the resultant wrench vector acting on the flotor is computed by summing the forces f_i and torques $FC_i \times f_i$, where f_i is computed by taking the vector product $I_i \times B_i$ of the current vectors $I_1, ..., I_6$ and the magnetic field vectors $B_1, ..., B_6$ (these are outward normals to the faces of the cube and are not drawn). These calculations are first done with respect to the vertex coordinate system $\{V, [i_V \;\; j_V \;\; k_V]\}$, then are transformed to the coordinate system $\{F, [i_F \;\; j_F \;\; k_F]\}$ located at the center of the cube and having k_F aligned with the vertical (in Figure 6 the plane of vertices V_A, V_B, V_C is horizontal). A resultant 6×6 matrix A mapping unit coil currents to flotor wrenches can be obtained from the device geometry, and the actuator force gain of 4 N/A predicted from calculations done later in the paper for

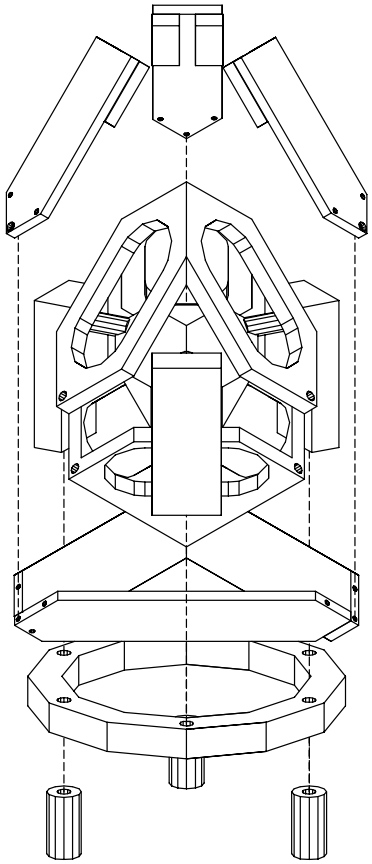

Figure 4: Haptic Interface Assembly Schematic

a coil resistance $R = 8\Omega$:

$$A = \begin{bmatrix} -1.15 & 2.31 & -1.15 & -3.46 & 3.46 & 0 \\ -2.00 & 0 & 2.00 & -2.00 & -2.00 & 4.00 \\ -3.27 & -3.27 & -3.27 & 0 & 0 & 0 \\ -0.10 & 0 & 0.10 & 0.03 & 0.03 & -0.07 \\ 0.06 & -0.12 & 0.06 & -0.06 & 0.06 & 0 \\ 0 & 0 & 0 & 0.09 & 0.09 & 0.09 \end{bmatrix}.$$

The first three rows of A have units of N/A, the next three Nm/A. It is worthwhile noting that A has two groups of *equal singular values* $5.66, 5.66, 5.66$ N/A and $0.16, 0.16, 0.16$ Nm/A corresponding to forces and torques, their scaled values giving the maximum forces and torques that would be obtained with a given power supply if all coil resistances were identical. Thus this geometry distributes the power load across the actuators in a uniform manner. With the optimized actuators used in this design, the power needed to actively levitate the cubic flotor and a handle attached to it (total mass 260 grams) is only $P_{lev} = 1.6$ W.

ACTUATOR OPTIMIZATION

Consider the actuator shown in Figure 5. Let d_c be the coil width, d the gap between the magnets, and $d_r = d - d_c$ the coil

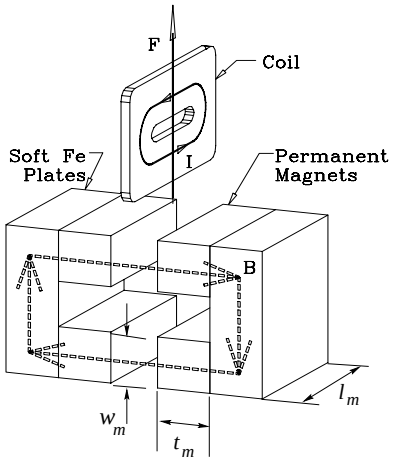

Figure 5: Basic Flat Coil Actuator

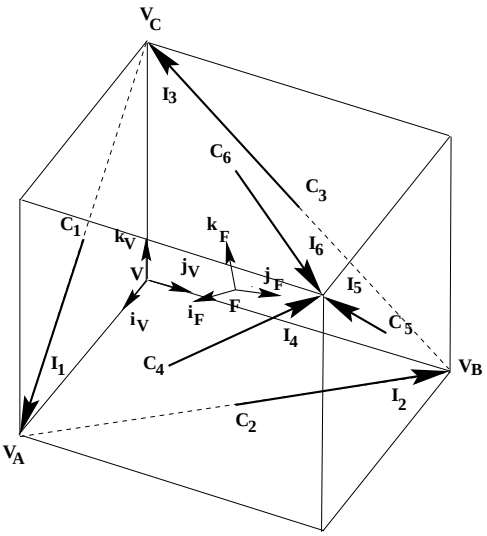

Figure 6: Coordinate assignments, coil centers and current vectors.

"rattle space". Let l_{wire} be the coil wire length, and η_{pack} be the coil "packing efficiency", i.e., $\eta_{pack} = s_{eff}/s_{wire}$, the ratio of conducting to total wire cross-sectional area. Note that η_{pack} depends on the wire cross-sectional shape (best packing achieved by flat wire), and the ratio of insulating material to conducting material. Let ρ be the coil conductor resistivity and R be the coil resistance. Let P_{coil} be the power dissipated in the coil, and let I be the coil current.

The actuator force is given by Lorentz's law. In obtaining the design formula (6) below, it is assumed that (i) the flux crossing the coil is a constant B_g, and, (ii) fringing fields are negligible, i.e., the flux outside the magnet projection through the coil is negligible. For the actuator in Figure 5, given assumption (ii), the length of wire that produces a force is given by $l_{eff} = 2l_m w_m d_c / s_{wire}$. Then, with $\eta_{geom} = 2l_m w_m d_c/(s_{wire} l_{wire})$ being an efficiency factor determined by the coil geometry, we ob-

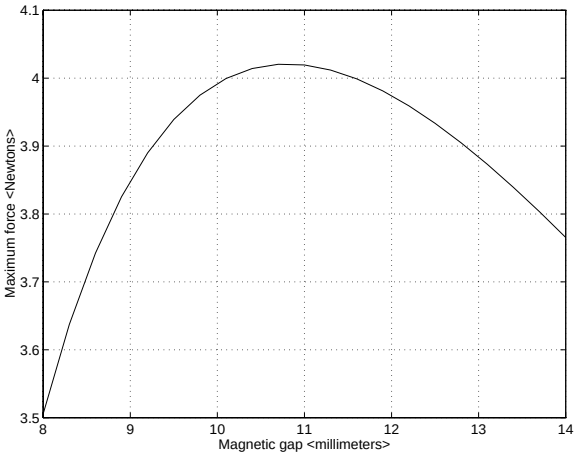

Figure 7: Actuator force *vs* gap with $d_r = 6$mm at $P_{coil} = 8$W ($l_m = 20$mm, $w_m = 8$mm, and $t_m = 4$mm), giving actuator gain at a current of 1A.

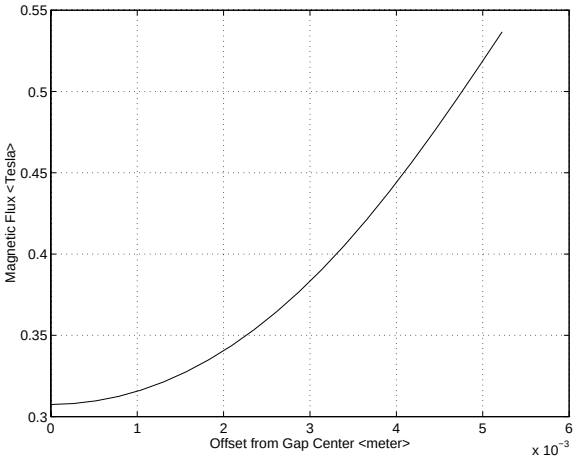

Figure 8: Predicted gap field at optimum gap (11mm)

tain the following expression for the actuator force:

$$F(B_g, d, l_m, w_m, t_m) = B_g\ I\ l_{eff} \tag{1}$$

$$= B_g \sqrt{\frac{P_{coil}}{R}}\ \frac{2 l_m w_m d_c}{s_{wire}} \tag{2}$$

$$= B_g \sqrt{\frac{P_{coil}}{\frac{\rho l_{wire}}{\eta_{pack} s_{wire}}}}\ \frac{2 l_m w_m d_c}{s_{wire}} \tag{3}$$

$$= B_g \sqrt{\eta_{pack}} \sqrt{\frac{P_{coil}}{\rho}} \sqrt{\frac{1}{s_{wire} l_{wire}}} 2 l_m w_m d_c \tag{4}$$

$$= B_g \sqrt{\eta_{pack}} \sqrt{\eta_{geom}} \sqrt{\frac{P_{coil}}{\rho}} \sqrt{2 w_m l_m d_c} \tag{5}$$

$$= B_g \sqrt{\eta_{pack}} \sqrt{\eta_{geom}} \sqrt{\frac{P_{coil}}{\rho}} \sqrt{2 w_m l_m (d - d_r)}\,. \tag{6}$$

For the coil shown in Figure 5, $\eta_{geom} \approx 2 l_m w_m / (2 l_m w_m + \pi w_m^2)$, and is approximately 0.6. Packing efficiencies for conventional (round copper wire) coils are about 75%, with flat copper coils reaching values close to 95%.

Assuming that the actuator flux in Figure 5 is steered perfectly by the soft iron back-plates, the field in the center of the gap aligned with the center of the magnet can be calculated by replacing the actuator magnets with equivalent solenoids and using the Biot-Savart Law. It is given by (Magnet Sales, 1996):

$$B_g(d, l_m, w_m, t_m) = \frac{2 B_r}{\pi} [\tan^{-1} \frac{w_m l_m}{d \sqrt{d^2 + l_m^2 + w_m^2}}$$

$$- \tan^{-1} \frac{w_m l_m}{(4 t_m + d) \sqrt{(4 t_m + d)^2 + l_m^2 + w_m^2}}]\ , \tag{7}$$

where B_r is the magnetic material residual flux. Substituting (7) in (6), one can relate the actuator dimensions to the resulting force. An additional lower bound of the form $t_s \geq \alpha w_m$ can be imposed on the iron return plates thickness in order to avoid saturation. With appropriate inequality constraints to account for the desired geometrical dimensions, *e.g.*, $2t_s + 2t_m + d \leq d_{max}$, t_m, w_m, l_m, and d that maximize actuator force can be obtained by solving a nonlinear program. The geometrical efficiency η_{geom} increases with the ratio l_m / w_m, while $l_m + 2 w_m$ will be bounded by flotor size. In practice, l_m, w_m are selected separately as a function of flotor geometry, desired motion and force range and desired force linearity. Then the magnet thickness t and the magnetic gap are selected by plotting the actuator force as a function of the magnetic gap d, as shown in Figure **??**, and choosing the maximizing d, i.e., *the best coil-width for a given rattle space.*

In this particular design, optimal actuator forces were calculated for a number of readily available magnet dimensions from plots such as the one shown in Figure 7. The dimensions $l_m = 20$mm, $w_m = 8$mm, and $t_m = 4$mm were selected as they show only a 25% loss of force relative to older designs (Hollis et. al., 1991),(Salcudean et. al., 1995) for the same power consumption, and over four times less magnetic material! Note that the coil width to gap ratio is substantially larger in this design then in all other reported designs (Hollis et. al., 1991),(Salcudean et. al., 1995),(Berkelman et. al., 1996). Furthermore, note that the above formulation does not involve the coil resistance, only the power dissipated in it, its resistivity and geometrical properties. Thus the coil resistance can be selected for maximum power transfer from the power amplifier *after* finding its dimensions. Not surprisingly, the wire gauge in this design was selected to give $R = 8\Omega$ in order to match available current drivers. Note that the predicted actuator force is correct only in the middle of the gap, when the flotor is in its nominal center. The magnetic field formula (7) can be extended to give the field along the magnet center line (Magnet Sales, 1996). The predicted curve for the optimal gap (11mm) obtained in Figure 7 is displayed in Figure 8. Note that the field increases near the magnets, giving a non-uniform force. This is averaged, to a certain extent, by the thick coil. Predicted force and field values have been compared to experimental ones with small errors (less than 5%) in several actuator designs of various sizes.

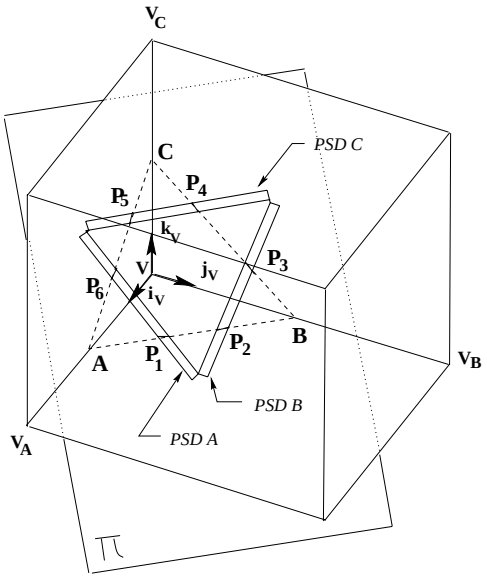

Figure 9: Optical sensor schematic

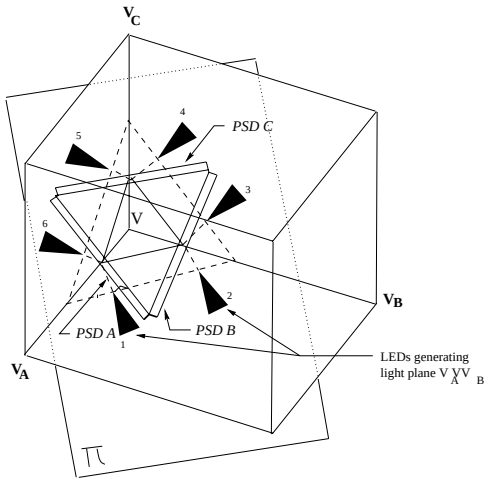

Figure 10: LED configuration for optical sensor

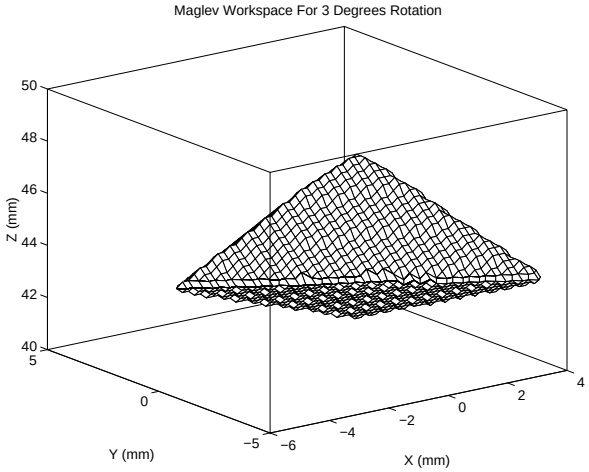

Figure 11: Optical sensor translational workspace for arbitrary rotations not exceeding 3°: the z-axis is the height of the vertex with respect to the PSD plane π

OPTICAL SENSOR

A novel optical sensor to compute the position and orientation offsets of the flotor with respect to the stator has been designed and fits under the horizontal coils of the flotor. Its schematic representation is shown in Figure 9. Three linear position sensing diodes (PSDs) are placed on a horizontal plane π under the flotor. The PSDs are mounted directly on the device PCB, so the plane π is the PCB plane translated upwards by the thickness of the PSDs. Three light planes V_AVV_B, V_BVV_C, and V_CVV_A, parallel to the flotor faces (here, for simplicity, schematically shown to coincide with the flotor faces) are generated by wide-angle infrared light emitting diodes (LEDs) attached to the flotor under the vertical coils and projecting infrared light through narrow slits towards the vertex V, as shown schematically in Figure 10. These light planes are turned on in sequence, first V_AVV_B, then V_BVV_C, then V_CVV_A, at high frequency, by the device microcontroller. When V_AVV_B is ON, the positions of the light spots P_1 and P_2 are detected by PSD A and PSD B, respectively, by measuring the PSD currents in synchronization with the flashed light plane. When V_BVV_C is ON, the light spot positions P_3 and P_4 are detected by PSD B and PSD C, respectively. When V_CVV_A is ON, the light spot positions P_5 and P_6 are detected by PSD C and PSD A, respectively.

When the flotor is in its nominal position with respect to the PSDs, points P_1 and P_6 collapse into one point, and so do the pairs P_2, P_3 and P_4, P_5 as shown in Figure 10. The position of the moving flotor with respect to a fixed coordinate system can be obtained from the plane π coordinates of the points P_i, $i = 1, ..., 6$, by first computing the intersections A of P_1P_2 with P_5P_6, B of P_1P_2 with P_3P_4, and C of P_3P_4 with P_5P_6, then by computing V as the point of intersection of three spheres of diameters $\|AB\|, \|BC\|, \|CA\|$. Indeed, the loci of V such that the angles $(\widehat{VA, VB})$, $(\widehat{VB, VC})$ and $(\widehat{VC, VA})$ are 90° are spheres with diagonals AB, BC and CA. Once V is located, $[i_V, j_V, k_V]$ can be computed by normalizing VA, VB, VC.

Note that similar sensors can be constructed by using three light planes that intersect three linear PSDs (or linear CCDs) and solving the associated direct kinematic equations numerically via an iterative method such as Newton's method. If the light planes are along the faces of a pyramid, the intersection of three thori needs to be computed.

This sensor has a number of advantages. Unlike prior LED-PSD-based sensors used in previous maglev wrists (Hollis et. al., 1991),(Berkelman et. al., 1996), only *linear*, not two-dimensional, PSDs are necessary. Since LEDs are inexpensive, cost savings for a similar measured volume are roughly one order of magnitude (the optical sensor described here costs roughly US$60 in quantities, while a sensor using two-dimensional PSDs would cost roughly US$600 in quantities, based on PSD prices from the same manufacturer). Since the PSDs are in the same

plane, they can be mounted on a single printed circuit board, with better alignement and manufacturability than would be the case if a three-dimensional PSD structure were used.

The sensor workspace is easy to quantify when the translation and rotation are decoupled. The translational workspace at null orientation is the union of two symmetrical pyramids, and becomes smaller as finite rotations of arbitrary axis are allowed (with PSDs with active areas of 24mm each, the horizontal side of the pyramid is roughly 22mm at null rotation). The semi-dextrous workspace volume showing the achievable translations for arbitrary axis flotor rotation of up to 3° is shown in Figure 11.

CONTROLLER BOARD

The controller board is a 10.6"x5" PCB comprising the following:
- analog electronics to amplify the PSD currents
- LED transistor drivers
- analog-to-digital converters to read the input from the PSDs, with enough spare channels to accommodate the outputs of a six-degree-of-freedom force sensor that could be mounted on the flotor
- Pulse-Width-Modulation (PWM)-driven H-bridges for the coils (3A continuous, 6A for 200ms peaks, max forces and acceleration mentioned in the abstract and conclusion based on these specs and a 48 V external power supply).
- one small fan for occasional forced air cooling,
- two serial and one parallel communication ports. The serial port can be used as a fast synchronous link allowing real-time control by a remote host. A second serial port is provided for the use of debugging tools. Several host communication methods are being provided, even though they take a significant amount of PCB space, for flexibility and exploration of the best approach to host connection.
- a 50MHz Intel 80C196NU microcontroller with associated EPROM and RAM. The microcontroller performs basic I/O communications with a host. It generates the time-multiplexed light planes needed for optical sensing and the PWM signals needed to drive the coils, and it computes the basic control functions (direct kinematics, wrench vector computation according to a control law for mechanism emulation, and transformation of the control wrench into equivalent coil forces or currents).

The support posts shown in Figure 4 locate the stator relative to the PCB and sensor, closer to one of the PCB sides, thus allowing a tapered surface for the user's forearm and wrist to rest on.

The controller board has been built and its basic functions have been tested. The basic operation of the optical sensor has been successfully tested, although some changes are required to provide a uniform intensity light plane in order to achieve the best resolution. Current driver routines, communication routines for SGI machines and fixed point kinematics routines have also been written and tested, but to this date the flotor has not yet been "flown".

CONCLUSION

The design of a small motion-range 6-DOF haptic interface was presented, including novel geometry and packaging, optical sensor, and actuator optimization. It is envisaged that the device will be used as (i) an intelligent haptic interface emulating simple mechanisms from its own library or downloaded from the host computer, such as limit stops, gimbals, sliders, various friction forces and simple geometric constraints that can be computed using its fixed-point microcontroller, (ii) a "dumb" haptic interface or teleoperation master, with the microcontroller board acting as an input-output board and most calculations being performed by the host or another external computer. The former mode does not require high communication rates with the host computer, while the second one does, as low-level data such as stiffnesses and forces are being passed between the host and the microcontroller board.

The characteristics of the device are summarized in the following table:

Moving mass	260 grams
Motion range	± 3 mm, $\pm 5°$
Maximum acceleration	> 10 g
Maximum continuous force	16 N
Peak force	34 N
Power consumption for levitation	1.6 W
Optical sensor resolution	approx. 10 microns
Isotropic design	
Optical sensor one order of magnitude cheaper than used in previous designs	
Optimized actuator over 50% more efficient than in previous designs	
All electronics except power supply integrated in the base with a 10.5"x5.5" footprint	

Table 1: Summary of desk-top joystick characteristics.

The haptic interface has a motion range that exceeds that of the successful passive "Space Mouse"/"Logitech Magellan" 6-DOF joystick designed in Dr. G. Hirzinger's group at DLR (Dietrich and Plank, 1988),(Hirzingger et. al., 1992), has high acceleration and force capability, and fits, complete with all electronics and a microcontroller, into a small enclosure tapering down from a handle 5.5" high to a base roughly two thirds the size of a sheet of paper.

ACKNOWLEDGEMENTS

The authors wish to thank A. Kelley for early design and other discussions, S. Bachmann for help with the mechanical design and sensor testing, L. Welder for help with the board design, construction and debugging, and D. Fletcher and L. Kjolby for machining. The original controller board design was done by Y. Lehrer under the authors' supervision. This work is supported by the Canadian IRIS NCE project HMI-6 and an associated British Columbia Provincial Infrastructure grant.

REFERENCES

Berkelman, P.J., Butler, Z.H., Hollis, R.L., "Design of a hemispherical magnetic levitation haptic interface device," in *Proc. 1996 ASME IMECE*, vol. DSC-58, November 17-22 1996.

Dietrich J., Plank, G., "Optoelectronic System Housed in a Plastic Sphere," 1988. European Patent No. 0 240 023; US-Patent No. 4,785,180; JP-Patent No. 1 763 620.

Hayward, V., Astley, O.R., "Performance measures for haptic interfaces," in *Proc. ISRR*, p. (12 pages), 1995.

Hirzinger, G., Dietrich, J., Gombert, B., Heindl, J., Landzettel, K., Schott, J., "The sensory and telerobotic aspects of the space robot experiment ROTEX," in *Int. Symposium on Artificial Intelligence, Robotics and Automation in Space*, (Toulouse, Labege, France), Sept. 30- Oct. 2 1992.

Hollis, R.L., Salcudean, S.E., Allan, P.A., "A six degree-of-freedom magnetically levitated variable compliance fine motion wrist: Design, modelling and control," *IEEE Trans. Rob. Aut.*, vol. 7, pp. 320–332, June 1991.

Hollis, R.L., Salcudean, S.E., "Lorentz levitation technology: a new approach to fine motion robotics, teleoperation, haptic interfaces, and vibration isolation," in *Proc. 5th Intl. Symp. on Robotics Research*, (Hidden Valley, PA), p. (18 pages), October 1-4 1993.

Magnet Sales & MFG Co. 1996 Catalog, "High performance permanent magnets." 11248 Playa Court, Culver City, CA 90230.

Salcudean, S.E., Wong, N.M., Hollis, R.L., "Design and Control of a Force-Reflecting Teleoperation System with Magnetically Levitated Master and Wrist," *IEEE Trans. Rob. Aut.*, vol. 11, pp. 844–858, December 1995.

Stocco, L., Salcudean, S.E., "A coarse-fine approach to force-reflecting hand-controller design," in *Proc. 1996 IEEE Intl. Conf. Rob. Aut.*, (Minneapolis, MN), pp. 404–410, April 22-28 1996.